**REMARKS**

The Office Action of May 17, 2005, has been carefully studied. No claim is allowed. Claims 1-19 presently appear in this application and define patentable subject matter warranting their allowance. Reconsideration and allowance are hereby respectfully solicited.

Claims 1-13 have been rejected under 35 U.S.C. §112, first paragraph, for lack of enablement. The examiner states that applicant's arguments regarding the 112 first paragraph rejection are not considered to be persuasive for the following reasons. Applicant fails to provide information allowing the skill artisan to ascertain all photosensitizer molecules being used for photodynamic therapy and all the quenching molecules being able to regulate the phototoxicity of a photosensitizer molecule without undue experimentation. In the instant case only a limited number of photosensitizer molecules and a limited number of quenching photosensitizer molecule examples are set forth, thereby failing to provide sufficient working examples. It is noted that these examples are neither exhaustive nor define the class of compounds required. The pharmaceutical art is unpredictable, requiring that each embodiment to be individually assessed for physiological activity. The instant claims read on all "effector photosensitizing molecules" being used for photodynamic therapy and all "quenching photosensitizer

molecules" being used for regulating the localized phototoxicity of an effector molecule, necessitating an exhaustive search for the embodiment to practice the claimed invention without undue experimentation. This rejection is respectfully traversed.

As acknowledged previously by the examiner, the skill of those in the art of photosensitizers and photodynamic therapy is very high. From the guidance provided by the present specification on "competitive quenching", such persons of high skill in the art would be well enabled to ascertain pairs of effector and quenching photosensitizer molecules suitable for use in the presently claimed method without undue experimentation. The enablement requirement does not require those of skill in the art to ascertain all photosensitizer molecules suitable for use in the presently claimed method as long as they can readily ascertain pairs of effector and quenching photosensitizer molecules that would be suitable.

The present specification teaches, by using the verteporfin/hypericin effector/quenching photosensitizer pair as a preferred embodiment, that the wavelength absorption maxima in the visible range of the quenching photosensitizer (e.g., absorption at 545 and 590 nm for hypericin) should be distantly shorter relative to the effector photosensitizer (e.g., verteporfin with an absorption maxima of 690 nm for excitation). This would facilitate selective excitation of the effector

photosensitizer with light at wavelengths greater than 650 nm without photoactivating hypericin, which is functioning here as a quenching photosensitizer instead of as an effector photosensitizer. See the present specification at page 29, paragraph [0057]. Claim 1 is now amended to recite that the absorption spectrum of the quenching photosensitizer molecule falls below the wavelength range used to excite the effector photosensitizer so that the quenching photosensitizer molecule cannot be excited by the same wavelength range used to excite the effector photosensitizer.

Those of skill in the art would instantly recognize that direct excitation energy transfer from verteporfin to hypericin is unlikely because light absorption by vertporfin occurs at longer (lower energy) wavelengths, not shorter (higher energy) wavelengths. Therefore, the respective absorption maxima wavelengths of verteporfin and hypericin make the pair incompatible with energy transfer to hypericin, which has shorter (higher energy) absorption maxima than verteporfin. However, as taught in the present specification at page 14, paragraph [0031], the quenching photosensitizer possesses a lower red/ox potential compared to the effector photosensitizer, which would enable the quenching photosensitizer (i.e., hypericin, which has moderately low red/ox potentials of E1/V=-1.01 mEV and E2/V=-1.31 mEV to effectively absorb energy transferred from verteporfin to oxygen

to generate singlet oxygen and free radicals. This enables hypericin to act as both electron acceptor and donor, facilitating energy scavenging from verteporfin or even from bioenergized electron transfer reactions in the cell.

Paragraph [0053] of the present specification discloses that dimethyl tetrahydroxyhelianthrone (DTHe), an analog of hypericin, also exhibited competitive quenching activity, albeit less effectively than hypericin. Other suitable effector and quenching photosensitizer pairs can be readily found by those of skill in the art following the guidance provided by the present specification from the many families of photosensitizing molecules, such as porphyrins, porphines, chlorines, texphyrins, porphycenes, phthalocyanines, psoralenes, dianthroquinones, etc. There is extensive knowledge in the art of photosensitizers, as evidenced by the 1211 hits in the NCBI PubMed literature database for review articles that include the term "photosensitizer". Accordingly, the skill in this art is exceedingly high and those of skill can readily select an effector and quenching photosensitizer pair from the literature, particularly once the wavelength of excitation by a laser for photodynamic therapy is selected. For example, the photosensitizer 5,10,15,20-tetrakis (m-hydroxyphenyl) bacteriochlorin has an optimum wavelength for biological activation at 739 nm and is an example of an effector photosensitizer that can be used to induce photodynamic damage

(Rovers et al., *Photochem. Photobiol.*, 72(3):358-364, 2000, a copy of which is attached hereto). A potential quencher of this phototoxicity is cercosporin, which has an absorption maximum at 474 nm and no absorption at all above 600 nm (Bilski et al., *Photochem. Photobiol.* 71(2):129-134, 2000, a copy of which is attached hereto).

As those in the art are highly skilled and the art of photodynamic agents/photosensitizers is well developed, only routine experimentation is needed to determine what pairs of photosensitizers would be suitable as an effector and quenching photosensitizer pair, particularly if a source, such as a laser, with a specific wavelength is selected for use. The effector photosensitizer would then be selected with an absorption maxima to be close to the wavelength of the laser. A suitable quenching photosensitizer is also selected which has an absorption maxima and spectrum of significantly shorter wavelength and which has a red/ox potential lower than the selected effector photosensitizer.

Reconsideration and withdrawal of the rejection are therefore respectfully solicited.

In view of the above, the claims comply with 35 U.S.C. §112 and define patentable subject matter warranting their allowance. Favorable consideration and early allowance are earnestly urged.

Respectfully submitted,

BROWDY AND NEIMARK, P.L.L.C.
Attorneys for Applicant(s)

By 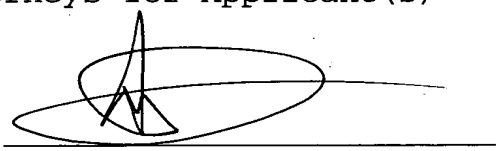
Allen C. Yun
Registration No. 37,971

ACY:pp
Telephone No.: (202) 628-5197
Facsimile No.: (202) 737-3528
G:\BN\N\nyum\Lavie7A\pto\amd OA 5-17-05.doc

Photochemistry and Photobiology, 2000, 72(3): 358–364

# *In Vivo* Photodynamic Characteristics of the Near-Infrared Photosensitizer 5,10,15,20-Tetrakis(*M*-Hydroxyphenyl) Bacteriochlorin¶

**Jeroen P. Rovers[1,2], Martin L. de Jode[1], Hadjira Rezzoug[1] and Michael F. Grahn*[1]**

[1]Academic Department of Surgery, Queen Mary and Westfield College, University of London, London, UK and
[2]Department of Surgery, Leiden University Medical Centre, Leiden, The Netherlands

**Received 9 March 2000; accepted 29 May 2000**

## ABSTRACT

**This paper describes the photodynamic characteristics of the new near-infrared photosensitizer 5,10,15,20-tetrakis(*m*-hydroxyphenyl)bacteriochlorin (mTHPBC or SQN400) in normal rat and mouse tissues. A rat liver model of photodynamic tissue necrosis was used to determine the *in vivo* action spectrum and the dose–response relationships of tissue destruction with drug and light doses. The effect of varying the light irradiance and the time interval between drug administration and light irradiation on the biological response was also measured in the rat liver model. Photobleaching of mTHPBC was measured and compared with that of its chlorin analog (mTHPC) in normal mouse skin and an implanted mouse colorectal tumor. The optimum wavelength for biological activation of mTHPBC in rat liver was 739 nm. mTHPBC was found to have a marked drug-dose threshold of around 0.6 mg $kg^{-1}$ when liver tissue was irradiated 48 h after drug administration. Below this administered drug dose, irradiation, even at very high light doses, did not cause liver necrosis. At administered doses above the photodynamic threshold the effect of mTHPBC–PDT was directly proportional to the product of the drug and light doses. No difference in the extent of liver necrosis produced by mTHPBC was found on varying the light irradiance from 10 to 100 mW $cm^{-2}$. The extent of liver necrosis was greatest when tissue was irradiated shortly after mTHPBC administration and necrosis was absent when irradiation was performed 72 h or later after drug administration, suggesting that the drug was rapidly cleared from the liver. In vivo photobleaching experiments in mice showed that the rate of bleaching of mTHPBC was approximately 20 times greater than that of mTHPC. It is argued that this greater rate of bleaching accounts for the higher photodynamic threshold and this could be exploited to enhance selective destruction of tissues which accumulate the photosensitizer.**

## INTRODUCTION

In recent years photodynamic therapy (PDT)† has emerged as a useful alternative to chemotherapy or radiotherapy in cancer treatment, offering improved selectivity due to preferential accumulation of the photosensitizing agent and controlled light delivery at the tumor. The effect of PDT depends on a multitude of parameters including the drug dose, light activation wavelength, light intensity, light dose and time interval between drug and light administration. As tissue optical properties and drug kinetics differ, each of these parameters needs to be optimized for each tissue or tumor type, which is not feasible in clinical trials. Thus, preclinical experiments in animal models are pivotal in the development of PDT regimens for a specific disease.

At present, we are investigating the potential of PDT as a minimally invasive treatment for tumors located within the liver. Previous studies have shown that PDT is capable of destroying tumor tissue within the liver completely with limited damage to the surrounding normal tissue (1,2). However, the photosensitizing agents used were excited with light of 630 to 652 nm, which has a limited penetration in most tissues (3). A photosensitizing agent which could solve this problem is 5,10,15,20-tetrakis(*m*-hydroxyphenyl)bacteriochlorin (mTHPBC or SQN400). It is the most highly reduced member of the tetrahydroxy phenyl porphyrin family of photosensitizers first synthesized by Bonnett (4,5). This compound differs from its chlorin analog temoporfin (mTHPC) only at a single bond, and so shares many of its chemical characteristics. However, in contrast to the chlorin which has a band I absorbance at 652 nm, mTHPBC has a very strong absorbance peak at 734 nm with a molar extinction coefficient of 139,000 $dm^3\ mol^{-1}\ cm^{-1}$ in methanol. This absorption peak shifts to about 740 nm in both aqueous solvents and tumor cells in cultures (6). In common with temoporfin, mTHPBC has a relatively low-fluorescence quantum yield (0.11) coupled with a high-triplet quantum yield (0.83) measured in methanol. The singlet-oxygen quantum yield varies from 0.43 in air saturated

¶ Posted on the website on 21 June 2000

*To whom correspondence should be addressed at: Academic Department of Surgery, The Royal London Hospital, Whitechapel, London E1 1BB, UK. Fax: +4420 7377 7283; e-mail: m.f.grahn@mds.qmw.ac.uk



†*Abbreviations:* ALSPc, aluminum chlorosulphonated phthalocyanine; Colo26, mice colon tumor cell line; DL-interval, time interval between drug administration and light irradiation; PDT, Photodynamic Therapy; mTHPBC, 5,10,15,20-tetrakis(*m*-hydroxyphenyl)bacteriochlorin (SQN400); mTHPC, 5,10,15,20-tetrakis(*m*-hydroxyphenyl)chlorin (temoporfin or Foscan®); PpIX, Protoporphyrin IX.

methanol to 0.62 in oxygen saturated methanol (7). Activation of mTHPBC at this near-infrared wavelength significantly increases light penetration, and thus treatment volumes, in most tissues (8).

When characterizing new photosensitizers for PDT it is important that the action spectrum is determined *in vivo* since the absorption maximum can depend strongly on the environment (9,10). The purpose of this study was to determine the optimum *in vivo* activation wavelength, the influence of drug dose, light dose, light intensity, and time interval between drug and light administration for mTHPBC in normal rat liver tissue. Experiments carried out *in vitro* suggest that mTHPBC is particularly susceptible to photobleaching (11) which might limit bioactivity. Because of this, the *in vivo* photobleaching of mTHPBC was assessed in an implanted tumor in the mouse.

## MATERIALS AND METHODS

*Animal models.* Male Wistar rats were used in all normal rat liver experiments. All animals were kept in standard cages with wood shavings as bedding and had free access to food and water. For all surgical procedures the animals were anaesthetized with a mixture of Hypnorm (Janssen Pharmaceutica, Tilburg, The Netherlands), Hypnovel (Roche, Hertfordshire, UK) and sterile water for injection (1:1:2, vol:vol:vol) at an intraperitonial dose of 2.7 ml $kg^{-1}$ body weight. To expose the liver a laparotomy was performed using a midline incision, and the liver was mobilized by cleavage of the falciform ligament.

Balb/c mice bearing the syngeneic mice colon tumor cell line (Colo26) adenocarcinoma were used in the photobleaching experiments. The Colo26 cells were grown in culture and implanted in the flank of female adult Balb/c mice as previously described (12). The photosensitizer was injected when the tumors had grown to an average diameter of 8 mm which is below the size at which central necrosis of the tumor occurs. For all procedures the mice were sedated using Hypnorm diluted 1:10 with sterile water for injection.

*Drugs.* The photosensitizers 5,10,15,20-tetrakis(*m*-hydroxyphenyl)chlorin (mTHPC or Foscan®) and mTHPBC were kindly donated by Scotia Pharmaceuticals (Stirling, UK). mTHPBC was dissolved in 1,2-propanediol/ethanol (6:4, vol/vol) and mTHPC in ethanol (96%)/polyethylene glycol 400/water (2:3:5, vol/vol/vol). Stock solutions were prepared freshly for each experiment. In all animals the photosensitizers were administered via the tail vein, after which the animals were kept under subdued light to prevent skin photodamage.

In vivo *action spectrum.* Rats were photosensitized by injection of mTHPBC at 0.5 mg $kg^{-1}$ 24 h prior to irradiation. To reduce the number of animals used, two measurements were obtained at different wavelengths using the two largest liver lobes in each animal. An Oxford Lasers CU15 copper vapor laser pumping a DL20 dye laser provided light at wavelengths between 727 and 747 nm. The dye used was a 1 m*M* solution in methanol of 1-ethyl-4-(4-(*p*-dimethylaminophenyl(-1,3-butadienyl)-pyridinium perchloracte, also known as Pyridine 2 or LDS 722 obtained from Exciton Inc. (Dayton, OH). A 1 cm diameter spot on each lobe was treated with 3 J $cm^{-2}$ light using a microlens (Type PTM-FD1, Medlight SA, Ecublens, Switzerland). This dose was chosen using data from pilot experiments to avoid full-thickness necrosis of the liver even when irradiation was close to the absorption peak for this photosensitizer. The wavelength of irradiation was verified using a portable monochromator (Optometrics UK Ltd., Leeds, UK) and was varied from 727 to 747 nm in 2 nm increments. Since the output power of the dye laser varied considerably with wavelength, it was always checked prior to irradiation. Because of this it was not possible to maintain a constant irradiance and this parameter varied between about 50 and 100 mW $cm^{-2}$ according to the wavelength. The exposure duration was adjusted to give the required light dose. The livers were harvested for assessment of the necrosis 48 h after irradiation. The depth of necrosis was measured directly on the excised livers along the plane of irradiation using Vernier calipers as described previously (13).

**Table 1.** Experiments on normal rat liver tissue using mTHPBC*

| Drug dose and Light dose experiments | N = | Irradiance experiments | N = | Drug-light interval experiments | N = |
|---|---|---|---|---|---|
| 0.1 mg $kg^{-1}$ | 5† | 2.5 J $cm^{-2}$ | 4‡ | 4 hours | 3§ |
| 0.3 | 5 | 5.0 | 4 | 24 | 3 |
| 0.6 | 5 | 10.0 | 4 | 48 | 3 |
| 1.2 | 5 | | | 72 | 3 |
| 2.4 | 5 | | | 120 | 3 |

* Table represents the different treatment groups and number of animals used per group as described in the text.
† Three different sites on the liver in one rat were irradiated with different light doses.
‡ Three different sites on the liver in one rat were irradiated with different light intensities.
§ Two different sites on the liver were irradiated, leading to 6 irradiations per treatment group.

*Drug and light dose experiments.* Animals were allocated to five groups of five rats each (Table 1) and injected with 0.1, 0.3, 0.6, 1.2 or 2.4 mg $kg^{-1}$ body weight mTHPBC 48 h prior to irradiation. At laparotomy the upper right, upper left and lower left lobe of the liver were exposed to 739 ± 3 nm light, generated by a diode laser (Applied Optronics Corporation, South Plainfield, NI USA), using a 1000 μm plain cut fiber in direct contact with the liver surface. The output power of the fiber was set to 100 mW and irradiations were performed for 25, 50 or 100 s to give a radiant energy of 2.5, 5 or 10 J, respectively. In an additional experiment two rats, administered 0.3 mg $kg^{-1}$ body weight mTHPBC, were irradiated for 200, 400 or 800 s to give a radiant energy of 20, 40 or 80 J, respectively. The livers were harvested for assessment of the necrosis 48 h after irradiation. The area of necrosis was determined by measurement of two diameters perpendicular to each other (R1 and R2) using Vernier calipers and subsequently calculated using the formula: ¼ π R1 R2.

*Irradiance experiments.* Animals were allocated to three groups of four rats each (Table 1) and injected with 1.0 mg $kg^{-1}$ body weight mTHPBC 24 h prior to irradiation. At laparotomy the upper right, upper left and lower left lobe of the liver were exposed to 739 nm light, generated by a diode laser (Applied Optronics Corporation). Each irradiation site was masked using a black cloth with a 5 mm hole cut in it, placed in contact with the liver surface. This allowed the irradiance to be varied by changing the distance between a microlens (Rare earth, W. Yarmouth, MA) and the liver surface. The laser output and spot size were adjusted to produce a surface irradiance of 10, 50 or 100 mW $cm^{-2}$ per site. Irradiation times were adjusted to give the same fluence per treatment site. Each group of rats received a different fluence, being 2.5, 5 or 10 J $cm^{-2}$. The livers were harvested for assessment of the necrosis 48 h after irradiation. The depth of necrosis was measured directly on the excised livers along the plane of irradiation using Vernier calipers.

*DL-interval experiments.* Animals were allocated to five groups of three rats each (Table 1) and injected with 1.0 mg $kg^{-1}$ body weight mTHPBC. At 4, 24, 48, 72 or 120 h after mTHPBC administration a laparotomy was performed and two sites on the liver were exposed to 739 nm light, generated by a diode laser (Applied Optronics Corporation), using a 1000 μm plain cut fiber in direct contact with the liver surface. The output power of the fiber was set to 100 mW and irradiations were performed for 100 s to give a radiant energy of 10 J. The livers were harvested for the assessment of the necrosis 48 h after irradiation. The area of necrosis was determined by measurement of two diameters perpendicular to each other (R1 and R2) using Vernier calipers and subsequently calculated using the formula: ¼ π R1 R2.

*In vivo photobleaching in tumor implanted in the mouse.* Tumor-bearing mice were given photosensitizer by intravenous injection into the tail vein 24 h before irradiation of the tumor. mTHPBC was given at a dose of 1.2 mg $kg^{-1}$ and mTHPC at a dose of 0.3 mg $kg^{-1}$. The fluorescence of each photosensitizer was measured using

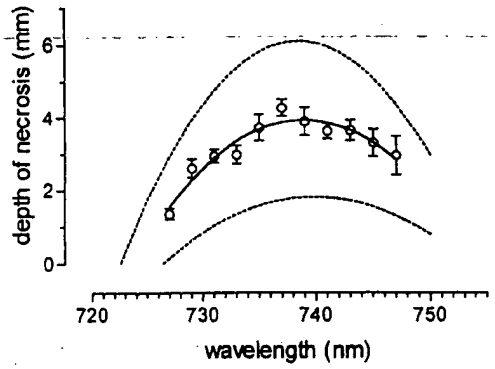


**Figure 1.** Action spectrum of mTHPBC in normal rat liver tissue. 24 h after mTHPBC administration (0.5 mg $kg^{-1}$) liver tissue was irradiated with light of a wavelength ranging from 727 nm to 747 nm with a 2 nm interval. The total light dose given was 3 J $cm^{-2}$ per wavelength. Data represent the mean ± SEM depth of necrosis within the liver, as assessed 48 h after light irradiation. The solid line represents a second order polynomial fit to the data, the dotted lines represent the extreme curves generated from the 95% confidence intervals of the second-order parameters derived from the curve fit.

a fiber optic probe placed onto the surface of the tumor before and during irradiation with light at 739 nm or 652 nm for mTHPBC and mTHPC, respectively. Fluorescence was excited using light at 418 nm for mTHPC and 514 nm for mTHPBC derived from a monocromated 100 W Xenon arc source (Applied Photophysics, London, UK). The fluorescence was detected using a monochromated CCD camera (Oriel Instaspec V). The system was calibrated and the data analyzed as described previously (14). The tumors were irradiated using light from diode lasers (Applied Optronics Corporation) at a fluence of 30 mW $cm^{-2}$ for both sensitizers. The irradiations were interrupted to allow the photosensitizer fluorescence to be measured. For mTHPBC the light was given in 7 s intervals to give 0.2 J $cm^{-2}$ between measurements, whilst for mTHPC light was given for 33 s intervals to give 1 J $cm^{-2}$ between measurements.

*Statistical analysis.* All values were expressed as mean ± SEM unless otherwise indicated. A one way ANOVA (with Bonferroni post-test) was used to evaluate differences in the extent of liver necrosis between the drug doses, light doses and light irradiances used in the experiments. A $P$-value of $< 0.05$ was considered to be statistically significant.

## RESULTS

### *In vivo* action spectrum

The variation of the depth of liver necrosis with the wavelength of the activating light is shown in Fig. 1. The form of the curve of depth of necrosis with wavelength will depend on a number of factors. These have been simplified by considering that the biological effect is the result of local singlet oxygen generation proportional to the number of photons absorbed by the photosensitizer. This depends on the fluence of light $\phi$ at wavelength $\lambda$, the concentration of the photosensitizer, and the absorption coefficient $\alpha(\lambda)$ of the photosensitizer at $\lambda$. Since PDT photonecrosis is a threshold phenomenon, necrosis only occurs when the amount of singlet oxygen exceeds this threshold. By making the reasonable assumption that the photosensitizer is evenly distributed throughout the liver tissue (on a macroscopic scale) and that the tissue optical properties remain constant for small deviations of wavelength from the optimum, then the zone of necrosis can be considered as the region of the liver in which

$$\alpha(\lambda)\,\phi(z) \geq q$$

where q is the threshold and

$$\phi(z) = \phi_0 \exp(-z/\delta)$$

$$\alpha(\lambda) = \alpha_0 \exp[-k(\lambda - \lambda_0)^2]$$

where k is a constant

Here the absorption of the photosensitizer in the proximity of the absorption peak has been modeled by a gaussian function. Hence, if the measured depth of necrosis at a particular wavelength is z

$$\alpha_0\,\phi_0 \exp[-k\,(\lambda - \lambda_0)^2 - z/\delta] = q$$

then

$$Z(\lambda) = \delta \log_e[(\alpha_0\phi_0)/q] - k\delta(\lambda - \lambda_0)^2$$

and since

$$Z_0 = \delta \log_e[(\alpha_0\,\phi_0)/q]$$

is a constant, the variation of necrosis depth (Z) with wavelength $\lambda$ in the region of the peak wavelength $\lambda_0$ is given by

$$Z(\lambda) = Z_0 - k\delta(\lambda - \lambda_0)^2$$

$$d_0 = k\delta(\lambda - \lambda_0)^2$$

which has the form of a second-order polynomial. The data were therefore fitted using a second-order polynomial to generate the solid curve shown in Fig. 1. The dotted lines represent the extreme curves generated from the 95% confidence intervals of the second-order parameters derived from the curve fit. The curve fit gives a value of 738.9 nm for the optimal wavelength of activation ($\lambda_0$) for mTHPBC with 95% confidence intervals of 738.5–739.9 nm.

### Effect of varying the drug dose

Figure 2a shows the area of PDT induced liver necrosis as a function of the mTHPBC dose administered. Irradiation of liver tissue after administration of 0.1 or 0.3 mg $kg^{-1}$ mTHPBC did not result in liver necrosis, regardless of the light dose given. In two rats administered 0.3 mg $kg^{-1}$ mTHPBC a light dose up to 80 J did not result in liver necrosis. However, an administered drug dose of 0.6 mg $kg^{-1}$ resulted in liver necrosis on irradiation. After 2.5 and 5 J of light liver necrosis in the 0.6 mg $kg^{-1}$ group was inhomogeneous; patches of white necrotic tissue were intermingled with apparently normal liver tissue. Liver necrosis after a light dose of 10 J and at higher drug doses was homogenous and lesions were circular in shape. In most cases necrosis extended throughout the entire thickness of the liver lobe. No damage to other organs was observed. The area of necrosis on the liver surface increased in a linear fashion with the administered drug dose for each light dose given, with significantly larger ($p < 0.01$) necrotic areas seen at the 2.4 mg $kg^{-1}$ dose than at the 0.6 mg $kg^{-1}$ dose for all radiant energies tested. The slopes of the linear fit were 27.6 ± 3.8, 41.4 ± 4.3 and 92.8 ± 11.1 $mm^2$ per mg $kg^{-1}$ for the 2.5, 5 and 10 J groups, respectively.

### Effect of varying the light dose

Figure 2b shows the area of PDT induced liver necrosis as a function of the given light dose (radiant energy). Once the

administered mTHPBC dose exceeded the phototoxic threshold, the extent of liver necrosis increased with increasing light energy. At each effective drug dose given there is a significant increase ($p < 0.01$) in the area of liver necrosis between a light dose of 2.5 and 10 J. At all effective drug doses administered the increase was linear, with a slope of 8.2 ± 0.8, 12.6 ± 0.9 and 20.5 ± 1.8 mm$^2$ J$^{-1}$ for an m-THPBC dose of 0.6, 1.2 and 2.4 mg kg$^{-1}$, respectively. These slopes were significantly different ($p < 0.05$) based on the 95% confidence intervals.

Figure 2c shows the area of necrosis as a function of the drug–light product. The drug–light product is calculated by multiplying the drug dose (mg kg$^{-1}$) with the light energy (J). There is a linear increase ($r^2 = 0.995$) in the area of necrosis with an increase in the drug–light product. The X-intercept of the linear fit is 0.52 mg J kg$^{-1}$.

### Effect of varying the light intensity (irradiance)

Table 2 shows the depth of liver necrosis after irradiation at different light irradiances. There was no significant difference ($p > 0.05$) between the mean depth of necrosis resulting from irradiation at 10, 50 or 100 mW cm$^{-2}$ light per given light energy (2.5, 5 or 10 J cm$^{-2}$). As would be expected, an increase in the total radiant energy given at any one irradiance resulted in a significant increase ($p < 0.05$) of the depth of necrosis from both 2.5 to 5.0 and 5.0 to 10 J cm$^{-2}$.

### Effect of varying the drug–light interval

Figure 3 shows the extent of PDT induced liver necrosis after light irradiation at different time intervals after m-THPBC administration. Necrotic lesions were clearly visible as homogeneous white, spherical lesions. Liver necrosis was full thickness in all cases, which made depth of necrosis unsuitable for comparison. The area of liver necrosis visible at the liver surface was largest when irradiation was performed 4 h after mTHPBC administration. Subsequently, the extent of necrosis decreased with an increase in the drug–light interval (DL-interval) and at a DL-interval of 72 and 120 h no liver necrosis was observed 2 days after light irradiation. In one animal at the 4 h DL-interval and one at the 24 h DL-interval damage to stomach and small bowel underneath the irradiated liver lobe was seen, indicating that the 739 nm light had penetrated beyond the liver.

### *In vivo* photobleaching of mTHPBC compared to mTHPC

The loss of photosensitizer fluorescence as a result of photobleaching during irradiation in tumors *in vivo* is shown in Fig. 4. The injected dose of bacteriochlorin was set at four times that of mTHPC in order to give a sufficient fluorescence signal for detection and to overcome the threshold for biological activity. It can be seen from the figure that m-THPBC is bleached considerably more rapidly than is m-THPC, and almost no photosensitizer fluorescence was detectable from the surface of the tumor after 30 s of irradiation. The ability of these doses of photosensitizer and light to induce tumor necrosis was confirmed in a separate group of animals. Eight mice were injected with 1.2 mg kg$^{-1}$ of

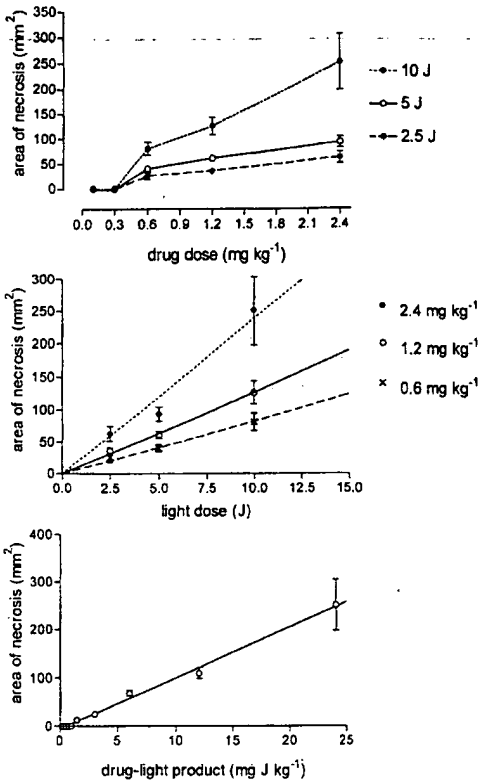


**Figure 2.** Effect of varying the drug dose and light dose on the extent of mTHPBC induced liver necrosis. Animals (n=5 per group) were administered a dose of 0.1, 0.3, 0.6, 1.2 or 2.4 mg kg$^{-1}$ m-THPBC via the femoral vein. Two days later three spots on the liver were irradiated with either 2.5, 5 or 10 J of 739 nm light at a fiber output of 100 mW. Data represent the mean ± SEM area of liver necrosis (mm$^2$) as a function of (a) the drug dose, (b) light dose or (c) drug–light product. Graph 2b only represents the drug dose groups that induced liver necrosis. The lines represent a linear fit of the individual data points, with a slope ± SEM of 8.2 ± 0.8, 12.6 ± 0.9 and 20.5 ± 1.8 for an mTHPBC dose of 0.6, 1.2 and 2.4 mg kg$^{-1}$ respectively. In graph 2c the line represents a linear fit of the means ($r^2 = 0.995$). The area of necrosis was calculated using the formula; ¼ π R1 R2, with R1 and R2 being the lesion diameters perpendicular to each other.

mTHPBC 24 h before irradiation with 3 J cm$^{-2}$ of 739 nm light at a surface irradiance of either 10 or 100 mW cm$^{-2}$. Full thickness necrosis of the tumors was seen in all the animals (tumor thickness ranged from 3.7 to 5.0 mm). By contrast, mTHPC injected into two groups of six mice at 0.5 mg kg$^{-1}$ one day before irradiation with 652 nm light at a surface irradiance of 30 or 150 mW cm$^{-2}$ resulted in an average of 3.9 ± 0.7 mm and 3.7 ± 0.8 mm of necrosis for the two irradiance levels, respectively.

## DISCUSSION

Bacteriochlorins are a promising class of photosensitizers for photodynamic therapy, as most of these compounds have a substantial absorption peak above 700 nm. Light at these near-infrared wavelengths penetrates tissues more deeply than the red light which has been used most often for PDT (3). This suggests that bacteriochlorins may be of particular

utility in the treatment of larger and more deeply seated tumors.

Our study showed that the optimal wavelength of activation for mTHPBC in normal rat liver tissue is 739 nm. Although there was considerable variation in the depth of necrosis between samples, reflecting differences in the tissue photosensitizer concentration between animals—leading to large confidence intervals in the parameter representing δ—there was considerably less uncertainty in the fit for the parameter representing $\lambda_0$, thus allowing a value for the optimal wavelength of activation to be obtained. This study indicates that for future clinical treatments with this photosensitizer a light source is required with a peak output within the range of 736–742 nm.

The effect of PDT treatment depends on a large number of parameters, of which the photosensitizer concentration, light dose and DL-interval are the most important. Tissue destruction in PDT occurs only when a minimum concentration of toxic photoproducts, such as singlet oxygen, is generated. This photodynamic threshold thus depends largely on the effective generation of singlet oxygen by the sensitizer and the amount of photosensitizer molecules present at the time of light irradiation.

The results of our study indicate that the photodynamic threshold of mTHPBC largely depends on the administered drug dose and thus the tissue concentration if one assumes that these show a linear correlation. Irradiation of liver tissue 48 h after administration of 0.1 or 0.3 mg $kg^{-1}$ mTHPBC did not result in liver necrosis, even when in the 0.3 mg $kg^{-1}$ drug dose group the light dose was increased up to 80 J. On the other hand, at an administered drug dose of 0.6 mg $kg^{-1}$ mTHPBC a light dose of only 2.5 J resulted in liver necrosis, although necrosis at this light dose was inhomogeneous. This suggests that the threshold for liver damage using mTHPBC is mainly determined by the tissue concentration and less by the light dose administered. For normal rat liver tissue a drug dose of at least 0.6 mg $kg^{-1}$ appears to be required to get liver necrosis upon light irradiation 48 h after drug administration. This is much greater than the threshold of mTHPC, since irradiation of rat liver 48 h after the administration of 0.1 mg $kg^{-1}$ mTHPC already leads to PDT damage (15).

**Table 2.** Effect of varying the light intensity on the extent of liver necrosis. Data represent the mean ± SEM depth of liver photonecrosis (mm) due to irradiation of mTHPBC sensitized liver tissue with 739 nm light. Animals (n = 12) were administered 1.0 mg $kg^{-1}$ and 24 hours later liver tissue was irradiated with an irradiance (E) of 10, 50 or 100 mW $cm^{-2}$ giving a total light fluence (ϕ) of 2.5, 5 or 10 J $cm^2$ (n = 4 per group). There is no significant difference in depth of necrosis between the different irradiances at a given fluence

| | ϕ | | |
|---|---|---|---|
| E (mW $cm^{-2}$) | 2.5 J $cm^{-2}$ | 5.0 J $cm^{-2}$ | 10 J $cm^{-2}$ |
| 10 | 3.0 ± 0.2 | 4.6 ± 0.1 | 5.2 ± 0.1 |
| 50 | 3.0 ± 0.1 | 4.4 ± 0.2 | 5.1 ± 0.2 |
| 100 | 3.5 ± 0.2 | 4.2 ± 0.2 | 4.6 ± 0.7 |

Previous *in vitro* experiments showed that mTHPBC was less phototoxic than mTHPC. This was attributed mainly to a reduced cellular uptake of mTHPBC and a reduced stability of the drug (unpublished data). The latter is mainly due to a high degree of photobleaching of mTHPBC. Bonnett *et al.* (11) showed that under air saturated conditions in solution mTHPBC was bleached much faster than mTHPC. The mouse tumor *in vivo* fluorescence measurements confirm that mTHPBC undergoes rapid photobleaching on irradiation. The exponential rate constants for the curve fits in Fig. 4 suggest that the initial rate of bleaching of mTHPBC is about 20 times that of mTHPC under similar conditions. This difference is greater than the seven-fold greater rate of bleaching for mTHPBC which we found for the photobleaching quantum yield of the two compounds in solution *in vitro* (unpublished data).

Photosensitizer photobleaching could well provide an explanation for the photodynamic threshold in general and specifically for the higher threshold of mTHPBC in rat liver tissue. The process of photobleaching will effectively reduce the amount of photosensitizer present in the tissue before enough reactive oxygen species are generated to give irreversible tissue damage. While this could be potentially disadvantageous for complete tumor eradication, it could also

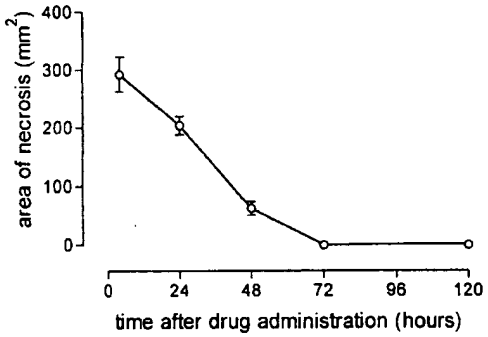


**Figure 3.** Effect of the DL-interval on the extent of mTHPBC-induced liver necrosis. Animals (n=5 per group) were irradiated 4, 24, 48, 72 or 120 h after administered of 1.0 mg $kg^{-1}$ mTHPBC. Liver tissue was irradiated with 100 mW of 739 nm light for 100 s, giving a total light dose of 10 J. Necrosis was assessed 48 h after light irradiation and areas calculated using the formula; ¼ π R1 R2, with R1 and R2 being the lesion diameters perpendicular to each other.

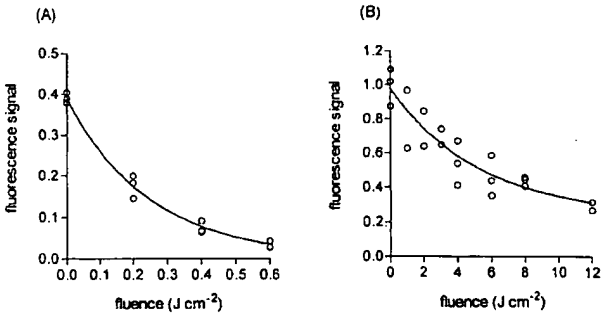


**Figure 4.** Photobleaching of photosensitizers in mouse tumor *in vivo*. Tumor bearing mice were injected with mTHPBC (A) and mTHPC (B) 24 h prior to irradiation with light at 739 or 652 nm light respectively. The graphs show triplicate determinations of the photosensitizer fluorescence measured on the tumor surface at intervals during the irradiation as described in the text. The solid lines represent an unconstrained single exponential fit to the data.

present a potential advantage. This would arise if drug levels in tumor surrounding normal tissue were reduced to below threshold levels due to the photobleaching process, preventing the occurrence of irreversible photodynamic damage. Photobleaching could thus be used to enhance treatment selectivity in PDT.

Once above threshold level the extent of mTHPBC-induced liver necrosis increases with both an increase in the drug dose and an increase in the light dose. In the range of drug doses tested in this study (0.1–2.4 mg $kg^{-1}$) there is a steady increase in the extent of necrosis with an increase in the drug dose. A linear fit of the data showed that the slopes of these linear curves differed with the applied light dose, indicating that the latter is also a contributing factor to the extent of necrosis. The linear increase in the extent of liver necrosis with administered drug dose indicates that at doses up to 2.4 mg $kg^{-1}$ of mTHPBC absorption of light by the photosensitizer does not limit light penetration, as has previously been shown for aluminum chlorosulfonated phthalocyanine (AlSPc) in normal rat liver (16). In theory, an increase in the drug dose would further increase the effect of PDT with mTHPBC. However, the use of increased drug doses is limited by the occurrence of unwanted effects, such as increased skin photosensitivity, which will be the limiting factor in setting the drug dose to be used for future clinical work.

At a constant irradiance the increase in the light dose led to a linear increase in the extent of liver necrosis. The slopes of the lines differed significantly between each given drug dose, indicating that drug dose is also a contributing factor, as discussed above. Over the range of light doses tested (2.5–10 J) the increase is linear. Similar findings have been reported for other photosensitizers (see, for example, van Gemert *et al.* (17) and Bown *et al.* (18). It should be noted that the form of the relationship between PDT necrosis and drug dose depends on the dimensions of the units used to express necrosis. Here we use $mm^2$ that results in a linear relationship. Measures of necrosis expressed in millimeters are best fitted by a log relationship. These findings support the theory that there is reciprocity between the drug dose and light dose, as has been described for other sensitizers both *in vitro* (19) and *in vivo* (20). However, at drug doses below the photodynamic threshold drug–light reciprocity fails, as is shown in our study. At an administered drug dose of 0.3 mg $kg^{-1}$ high light doses did not result in liver necrosis, which would have been expected if reciprocity were maintained. Fingar *et al.* (21) reported similar results with Photofrin where reciprocity failed at low drug levels and high light doses. Messmann *et al.* (22) attributed the breakdown of reciprocity to the photodegradation of Protoporphyrin IX (PpIX) during treatment, which could be equally true for the rapidly bleaching photosensitizer mTHPBC used in our study. Due to the drug–light reciprocity the drug–light product could be a useful tool in treatment planning, once photosensitizer tissue concentrations above the photodynamic threshold are guaranteed.

It has been suggested that the use of light at low intensities improves tumor responses to PDT (23,24). This effect has mainly been attributed to the maintenance of tumor oxygenation during treatment with low fluence rates (25). In contrast with tumor tissue, the PDT effect in normal tissues often appears to be fluence rate independent (26,27). This is in concordance with the results of this study, which shows no difference in the extent of liver necrosis at high or low light irradiances. This difference is attributed to the better blood supply of normal tissue versus tumor tissue, making it less probable that tissue oxygen is completely depleted during PDT in normal tissue (28).

Although low fluence rates have shown to improve tumor responses to PDT, longer light irradiation times are required to achieve equivalent tumor responses as to high fluence rates (29) and they could reduce treatment selectivity (30). When clinically applied, short light irradiation times are preferred and thus higher fluence rates will be more applicable.

Of utmost importance in PDT is the time interval between drug administration and light irradiation. In treatment of cancerous lesions the DL-interval will determine the selectivity of the PDT treatment, as a difference in tissue kinetics will in most cases lead to preferential tumor tissue concentrations at later time intervals (31,32). Irradiation of mTHPBC sensitized normal rat liver tissue showed a maximum amount of necrosis when irradiated 4 h after mTHPBC administration. The extent of necrosis decreased subsequently with time after drug administration. Irradiation at 72 and 120 h after mTHPBC administration did not result in liver necrosis, indicating that tissue drug levels have fallen below threshold levels at these time intervals. The bioactivity kinetics of mTHPBC in normal liver seem to resemble those of m-THPC, with the high drug levels found shortly after drug administration after which the concentration steadily decreases (33). On the basis of the time course of mTHPBC bioactivity, we believe it is safe to assume that mTHPBC drug levels will show a similar kinetic pattern. In conclusion, in normal rat liver tissue mTHPBC is optimally activated in the near-infrared region at a wavelength of 739 ± 1 nm. Once the photodynamic threshold has been exceeded the extent of liver necrosis increases with both drug dose and light dose, as shown by the good correlation of liver necrosis with the drug–light product. Changing the light intensity over the range tested does not influence the extent of normal liver necrosis with mTHPBC. The extent of liver necrosis depends largely on the time interval between drug administration and light irradiation, with a decrease in the extent of liver necrosis in time. Maximum liver necrosis is induced when tissue is irradiated shortly after administration of the maximum tolerated dose of mTHPBC with the highest light dose possible with respect to clinically practical treatment times. Future studies on tumor models are required to assess the efficacy of mTHPBC–PDT in the treatment of intrahepatic tumors.

*Acknowledgments*—We gratefully acknowledge the support of Scotia Pharmaceuticals Ltd. (Stirling, UK) for JPR (student grant).

## REFERENCES

1. van Hillegersberg, R., J. P. Marijnissen, W. J. Kort, P. E. Zondervan, O. T. Terpstra and W. M. Star (1992) Interstitial photodynamic therapy in a rat liver metastasis model. *Br. J. Cancer* **66**, 1005–1014.
2. Rovers, J. P., J. J. Schuitmaker, A. L. Vahrmeijer, J. H. van Dierendonck and O. T. Terpstra (1998) Interstitial photodynamic therapy with the second-generation photosensitizer bacteriochlorin a in a rat model for liver metastases. *Br. J. Cancer* **77**, 2098–2103.

3. Wilson, B. C., W. P. Jeeves, D. M. Lowe and G. Adam (1984) *Light propagation in animal tissues in the wavelength range of 375–825 nanometers. Porphyrin localization and treatment of tumors*, pp. 115–132. Liss, New York.
4. Berenbaum, M. C., S. L. Akande, R. Bonnett, H. Kaur, S. Ioannou, R. D. White and U. J. Winfield (1986) meso-Tetra-(hydroxyphenyl)porphyrins, a new class of potent tumor photosensitisers with favourable selectivity. *Br. J. Cancer* **54**, 717–725.
5. Bonnett, R., R. D. White, U. J. Winfield and M. C. Berenbaum (1989) Hydroporphyrins of the meso-tetra(hydroxyphenyl)porphyrin series as tumor photosensitizers. *Biochemical Journal* **261**, 277–280.
6. Grahn, M. F., A. McGuinness, R. Benzie, R. Boyle, M. L. de Jode, M. G. Dilkes, B. Abbas and N. S. Williams (1997) Intracellular uptake, absorption spectrum and stability of the bacteriochlorin photosensitizer 5, 10, 15, 20-tetrakis(m-hydroxyphenyl)bacteriochlorin (mTHPBC) Comparison with 5, 10, 15, 20-tetrakis(m-hydroxyphenyl)chlorin (mTHPC) *J. Photochem. Photobiol. B Biol.* **37**, 261–266.
7. Bonnett, R., P. Charlesworth, B. D. Djelal, S. Foley, D. J. McGarvey and T. G. Truscott (1999) Photophysical properties of 5, 10, 15, 20-tetrakis(*m*-hydroxyphenyl)porphyrin (m-THPP), 5, 10, 15, 20-tetrakis(*m*-hydroxyphenyl)chlorin (m-THPC) and 5, 10, 15, 20-tetrakis(*m*-hydroxyphenyl)bacteriochlorin (m-THPBC): a comparative study. *J. Chem. Soc. Perkin Trans.* **2**, 325–328.
8. Rovers, J. P., M. L. de Jode and M. F. Grahn (2000) Significantly increased laser light-induced damage using the near-infra red photosensitizer 5, 10, 15, 20-tetrakis(*m*-hydroxyphenyl) bacteriochlorin in interstitial photodynamic therapy of normal rat liver tissue. *Lasers Surg. Med.* (In press).
9. Star, W. M (1995) In vivo action spectra, absorption and fluorescence excitation spectra of photosensitizers for photodynamic therapy. *J. Photochem. Photobiol. B Biol.* **28**, 101–102.
10. Anderson, V. C. and D. H. Thompson (1992) Triggered release of hydrophilic agents from plasmalogen liposomes using visible light or acid. *Biochim. Biophys. Acta* **1109**, 33–42.
11. Bonnett, R., B. D. Djelal, P. A. Hamilton, G. Martinez and F. Wierrani (1999) Photobleaching of 5,10,15,20-tetrakis(m-hydroxyphenyl)porphyrin (mTHPP) and the corresponding chlorin (mTHPC) and bacteriochlorin (mTHPBC) A comparitive study. *J. Photochem. Photobiol. B Biol.* **53**, 136–143.
12. Ansell, J. K., M. L. de Jode and M. F. Grahn (1997) Characterisation of a murine model for the rapid assessment of the acute photodynamic response in tumor and muscle. *Lasers Med. Sci.* **12**, 336–341.
13. de Jode, M. L., J. A. McGilligan, M. G. Dilkes, I. Cameron, M. F. Grahn and N. S. Williams (1996) An in vivo comparison of the photodynamic action of a new diode laser and a copper vapour dye laser at 652 nm. *Lasers Med. Sci.* **11**, 117–121.
14. Grahn, M. F., M. L. de Jode, M. L. Dilkes, J. K. Ansell, D. Onwu, J. Maudsley and N. S. Williams (1997) Tissue photosensitizer detection by low-power remittance fluorimetry. *Lasers Med. Sci.* **12**, 245–252.
15. Rovers, J. P., A. E. Saarnak, A. Molina, J. J. Schuitmaker, H. J. C. M. Sterenborg and O. T. Terpstra (1999) Effective treatment of liver metastases with photodynamic therapy, using the second generation photosensitizer meta-tetra(hydroxyphenyl)-chlorin (mTHPC), in a rat model. *Br. J. Cancer* **81**, 600–608.
16. Wilson, B. C., M. S. Patterson and D. M. Burns (1986) Effect of photosensitizer concentration in tissue on the penetration depth of photoactivating light. *Lasers Med. Sci.* **1**, 235–244.
17. van Gemert, J. C., M. C. Berenbaum and G. H. M. Gijsberg (1985) Wavelength and light-dose dependence in tumor photo-therapy with hematoporphyrin derivative. *Br. J. Cancer* **52**, 43–49.
18. Bown, S. G., C. J. Tralau, P. D. Smith, D. Akdemir and T. J. Wieman (1986) Photodynamic therapy with porphyrin and phthalocyanine sensitisation: quantitative studies in normal rat liver. *Br. J. Cancer* **54**, 43–52.
19. Gibson, S. L. and S. Hilf (1985) Interdependence of fluence, drug dose and oxygen on hematoporphyrin derivative induced photosensitization of tumor mitochondria. *Photochem. Photobiol.* **42**, 367–373.
20. Cowled, P. A. and I. J. Forbes (1985) Photocytotoxicity in vivo of hematoporphyrin derivative components. *Cancer Lett.* **28**, 111–118.
21. Fingar, V. H., W. R. Potter and B. W. Henderson (1987) Drug and light dose dependence of photodynamic therapy: a study of tumor cell clonogenicity and histologic changes. *Photochem. Photobiol.* **45**, 643–650.
22. Messmann, H., P. Mlkvy, G. Buonaccorsi, C. L. Davies, A. J. MacRobert and S. G. Bown (1995) Enhancement of photodynamic therapy with 5-aminolaevulinic acid-induced porphyrin photosensitisation in normal rat colon by threshold and light fractionation studies. *Br. J. Cancer* **72**, 589–594.
23. van Geel, I. P., H. Oppelaar, J. P. Marijnissen and F. A. Stewart (1996) Influence of fractionation and fluence rate in photodynamic therapy with Photofrin or mTHPC. *Radiat. Res.* **145**, 602–609.
24. Rezzoug, H., O. Bezdetnaya, O. A'Amar, F. Merlin and F. Guillemin (1998) Influence of different parameters on photodynamic activity of meso-tetra(m-hydroxyphenyl)chlorin (m-THPC): *in vitro* and *in vivo*. *Lasers Med. Sci.* **13**, 119–125.
25. Foster, T. H., R. S. Murant, R. G. Bryant, R. S. Knox, S. L. Gibson and R. Hilf (1991) Oxygen consumption and diffusion effects in photodynamic therapy. *Radiation Research* **126**, 296–303.
26. Gomer, C. J., N. Rucker, N. J. Razum and A. L. Murphree (1985) In vitro and in vivo light dose rate effects related to hematoporphyrin derivative photodynamic therapy. *Cancer Res.* **45**, 1973–1977.
27. Chen, Q., M. Chopp, M. O. Dereski, B. C. Wilson, M. S. Patterson, A. Schreiber and F. W. Hetzel (1992) The effect of light fluence rate in photodynamic therapy of normal rat brain. *Radiation Research* **132**, 120–123.
28. Tromberg, B. J., A. Orenstein, S. Kimel, S. J. Barker, J. Hyatt, J. S. Nelson and M. W. Berns (1990) In vivo tumor oxygen tension measurements for the evaluation of the efficiency of photodynamic therapy. *Photochem. Photobiol.* **52**, 375–385.
29. Sitnik, T. M. and B. W. Henderson (1996) The effect of fluence rate on tumor and normal tissue responses to photodynamic therapy. *Photochem. Photobiol.* **67**, 462–466.
30. Andrejevic-Blant, S., A. Woodtli, G. Wagnieres, C. Fontolliet, H. van den Bergh and P. Monnier (1996) In vivo fluence rate effect in photodynamic therapy of early cancers with tetra(m-hydroxyphenyl)chlorin. *Photochem. Photobiol.* **64**, 963–968.
31. Stewart, F. A. and Y. Oussoren (1993) Functional and histological bladder damage in mice after photodynamic therapy: the influence of sensitiser dose and time of administration. *Br. J. Cancer* **68**, 673–677.
32. van den Boogert, J., R. van Hillegersberg, H. J. van Staveren, R. W. F. de Bruin, H. van Dekken, P. D. Siersema and H. W. Tilanus (1999) Timing of illumination is essential for effective and safe photodynamic therapy: a study in the normal rat oesophagus. *Br. J. Cancer* **79**, 825–830.
33. Rovers, J. P., A. E. Saarnak, M. de Jode, H. J. C. M. Sterenborg, O. T. Terpstra and M. F. Grahn (2000) Biodistribution and bioactivity of tetra-pegylated meta-tetra(hydroxyphenyl)chlorin compared to native meta-tetra(hydroxyphenyl)chlorin in a rat liver tumor model. *Photochem. Photobiol.* **77**, 210–217.

Photochemistry and Photobiology, 2000, 71(2): 129–134

## Symposium-in-Print

# Vitamin $B_6$ (Pyridoxine) and Its Derivatives Are Efficient Singlet Oxygen Quenchers and Potential Fungal Antioxidants

**P. Bilski*[1], M. Y. Li[1], M. Ehrenshaft[2], M. E. Daub[2] and C. F. Chignell[1]**

[1]Laboratory of Pharmacology & Chemistry, NIEHS Environmental Toxicology Program, NC, USA and
[2]Department of Plant Pathology, North Carolina State University, Raleigh, NC, USA

**Received 30 July 1999; accepted 19 October 1999**

## ABSTRACT

**Vitamin $B_6$ (pyridoxine, 1) and its derivatives: pyridoxal (2), pyridoxal 5-phosphate (3) and pyridoxamine (4) are important natural compounds involved in numerous biological functions. Pyridoxine appears to play a role in the resistance of the filamentous fungus *Cercospora nicotianae* to its own abundantly produced strong photosensitizer of singlet molecular oxygen ($^1O_2$), cercosporin. We measured the rate constants ($k_q$) for the quenching of $^1O_2$ phosphorescence by 1–4 in $D_2O$. The respective total (physical and chemical quenching) $k_q$ values are: 5.5 × $10^7$ $M^{-1}$ $s^{-1}$ for 1; 7.5 × $10^7$ $M^{-1}$ $s^{-1}$ for 2, 6.2 × $10^7$ $M^{-1}$ $s^{-1}$ for 3 and 7.5 × $10^7$ $M^{-1}$ $s^{-1}$ for 4, all measured at pD 6.2. The quenching efficacy increased up to five times in alkaline solutions and decreased ~10 times in ethanol. Significant contribution to total quenching by chemical reaction(s) is suggested by the degradation of all the vitamin derivatives by $^1O_2$, which was observed as declining absorption of the pyridoxine moiety upon aerobic irradiation of RB used to photosensitize $^1O_2$. This photodegradation was completely stopped by azide, a known physical quencher of $^1O_2$. The pyridoxine moiety can also function as a redox quencher for excited cercosporin by forming the cercosporin radical anion, as observed by electron paramagnetic resonance. All $B_6$ vitamers fluoresce upon UV excitation. Compounds 1 and 4 emit fluorescence at 400 nm, compound 2 at 450 nm and compound 3 at 550 nm. The fluorescence intensity of 3 increased ~10 times in organic solvents such as ethanol and 1,2-propanediol compared to aqueous solutions, suggesting that fluorescence may be used to image the distribution of 1–4 in *Cercospora* to understand better the interactions of pyridoxine and $^1O_2$ in the living fungus.**

*To whom correspondence should be addressed at: Environmental Toxicology Program, National Institute of Environmental Health Sciences, National Institutes of Health, P.O. Box 12233, Research Triangle Park, NC 27709, USA. E-mail: Bilski@niehs.nih.gov



## INTRODUCTION

The term vitamin $B_6$ is used to describe all biologically interconvertable forms of pyridoxine that include pyridoxine, pyridoxal, pyridoxal 5-phosphate and pyridoxamine. Vitamin $B_6$ is an essential co-factor in numerous enzymatic reactions involved primarily in amino acid metabolism. All living organisms require vitamin $B_6$ and they must either synthesize it or, like humans, derive it from nutrients. In addition to its role as a vital co-factor, our recent findings (1) suggest that vitamin $B_6$ may function as an antioxidant by interacting with singlet molecular oxygen during (photo)oxidative stress in the filamentous fungus *Cercospora nicotianae*. The wild-type strain of this fungus produces and is highly resistant to the potent photosensitizer cercosporin and is also highly resistant to other singlet oxygen photosensitizers of diverse structure and solubility.

Production of *C. nicotianae* mutant strains (2,3) sensitive to both cercosporin and other photosensitizers led to the identification of a gene apparently required for the resistance exhibited by the wild-type strain (4,5). Further characterization of this gene (1) revealed that it encoded a component necessary for pyridoxine synthesis in *C. nicotianae* as well as in other organisms and that pyridoxine and its derivatives are capable of quenching singlet oxygen *in vitro*. Other vitamins such as vitamin C and vitamin E are powerful antioxidants and scavengers of active oxygen species including singlet oxygen, but the ability of vitamin $B_6$ to quench singlet oxygen had not previously been reported.

Singlet oxygen ($^1O_2$) is a strong oxidizer and a potent initiator of radical oxidation in biological systems. It is best detected by its infrared phosphorescence at 1270 nm, which, although difficult to measure, is very specific for $^1O_2$ and is usually free of spectral interference from other emissions. The phosphorescence is quenched by antioxidants, and the rate constants for this quenching may be a direct and convenient measure of an antioxidant potential. We measured the rate constants for $^1O_2$ quenching by pyridoxine and its derivatives, and found that they are strong quenchers and good substrates for $^1O_2$, especially in an aqueous environment. We also characterized pyridoxine fluorescence that may help to determine the distribution of pyridoxine in the fungus by fluorescence microscopy.

## MATERIALS AND METHODS

*Chemicals.* Ethanol, 1,4-dioxane, 1,2-propanediol (all spectrophotometric grade), Triton X-100, rose bengal (RB) † and 5,5-dimethyl-1-pyrroline *N*-oxide (DMPO) were purchased from Aldrich Chemical Co. (Milwaukee, WI). The DMPO was vacuum distilled and stored at −20°C. Deuterium oxide was from Cambridge Isotope Laboratories (Andover, MA). The pyridoxine vitamers and surfactant benzalconium chloride were purchased from Sigma Chemical Co. (St. Louis, MO). Cercosporin was extracted from cultures of *Cercospora kikuchii* strain PR as previously described (6). All experiments were performed using freshly prepared air-equilibrated solutions at room temperature.

*Absorption and fluorescence spectra.* Absorption spectra were measured using an HP diode array spectrophotometer model 8452A (Hewlett Packard Co., Palo Alto, CA). Fluorescence spectra were recorded on an SLM SPC 823-SMC 220 spectrofluorometer (SLM Instruments, Urbana, IL) as described previously (7). The relative number of absorbed photons at the excitation wavelength was calculated using the Beer–Lambert law.

*Singlet oxygen detection.* Singlet oxygen phosphorescence was recorded on a steady-state $^1O_2$ spectrophotometer (8) featuring an optimized optical system as in our pulse $^1O_2$ spectrophotometer (9). Samples were excited from a 500 W mercury lamp operating at 300 W through appropriate filter(s). The $^1O_2$ phosphorescence spectra were recorded over the range of 1200–1350 nm and were normalized to the same number of absorbed photons (10) at the excitation wavelength.

Singlet oxygen lifetimes were measured using a laser pulse spectrometer described in detail elsewhere (9). In this study, the apparatus utilized a Surelite II laser (Continuum, Santa Clara, CA) for excitation. A germanium diode (model 403 HS, Applied Detector Corporation, Fresno, CA) in conjunction with an efficient optical system was used for signal detection. Data were acquired on an HP 54111d digitizing oscilloscope (Hewlett Packard, Colorado Springs, CO) interfaced to a PC computer. Singlet oxygen was produced by single pulse excitation at 532 nm of RB as a photosensitizer. The $^1O_2$ lifetime was calculated from a monoexponential decay of its phosphorescence.

*Oxidation of pyridoxine derivatives.* Oxidation of pyridoxine derivatives by $^1O_2$ was performed at 25°C using a 450 W xenon–mercury lamp and a combination of a cutoff filter (400 nm) and an interference filter (548 nm) for RB excitation. The sample was placed in a closed 1 cm pathlength cuvette and was stirred during irradiation. The absorption spectra were taken at appropriate intervals to obtain up to a 50% decrease in pyridoxine absorption due to photooxidation while the absorption spectrum of RB was unchanged. The photooxidation rate was normalized, if necessary, using the number of photons absorbed by RB, allowing quantitative interpretation of photooxidation data (7,10).

The initial rates of oxidation were taken for calculations that were performed assuming a steady-state approximation for $^1O_2$ production and decay. The relative rate constant values, $k_r(\text{rel}) = I_x\varphi_{\Delta x}k_r(P)$ were calculated from the initial consumption rates assuming 1:1 stoichiometry for consumed oxygen and decayed vitamer. The following equation was applied (11):

$$\frac{r(k_d + k_q[P_o])}{[P_o]} = I\varphi_\Delta k_r^{[P]}$$

where r is the measured oxidation rate; $k_d$, the rate constant of the natural $^1O_2$ decay; $k_q$, the measured total (chemical plus physical) $^1O_2$ quenching rate constant; $[P_0]$, the initial concentration of pyridoxine substrate; I, the irradiation rate for photons absorbed by RB (not measured here); and $\varphi_\Delta$, the quantum yield of $^1O_2$ production. The values of $k_d$ and $k_q$ were measured in separate experiments in $D_2O$ solutions (Table 1). Because the $I\varphi_\Delta$ factor was constant in all experiments, $k_r$(rel) values allow a direct comparison of the oxication efficacy for all $B_6$ vitamers.

*Electron paramagnetic resonance (EPR) measurements.* The EPR spectra were measured using an X-band E-Line Century Series EPR spectrometer (Varian, Palo Alto, CA) equipped with a TM110 cavity. Samples were irradiated directly inside the microwave cavity of the spectrometer with light from a 1 kW xenon lamp (Krotos) after passing through a cutoff filter transmitting above 300 nm. Spectra were accumulated on a PC and stimulated using software described elsewhere (12).

†*Abbreviations:* DMPO, 5,5-dimethyl-1-pyrroline *N*-oxide; EPR, electron paramagnetic resonance; RB, rose bengal.

## RESULTS AND DISCUSSION

The structures of pyridoxine (**1**), pyridoxal (**2**), pyridoxal 5-phosphate (**3**) and pyridoxamine (**4**) are shown in Scheme 1. The vitamers have pH-sensitive groups and the reported pKa values (13) are as follows: 5.0 and 8.96 for **1**; 4.2 and 8.66 for **2**; 2.5, 4.14, 6.2 and 8.69 for **3**; and 3.37, 8.01 and 10.13 for **4**. While it may be expected that pH will influence the spectral and photochemical properties of these vitamers, we mostly focused our attention on the physiologically relevant pH values (Table 1). All vitamers can exist in several ionization forms that may interact differently with singlet oxygen, and there will be a contribution from more than one species at physiological pH. As we feel that the dissociation of the –OH group has the potential to influence greatly the charge density on the pyridoxine ring (and subsequent interaction with $^1O_2$) we did not assign the quenching or oxidation rates to a particular ionic species. We believe that the experimentally observed values are sufficient and more relevant to explain the vitamins' oxidation under physiologically relevant conditions.

### Absorption and fluorescence

Information on the absorption and fluorescence properties was needed to select suitable conditions for photochemical experiments with the $B_6$ vitamers. In addition, differences in the intensity and/or position of the spectra in different chemical environments will have utility in determining vitamer localization in the *Cercospora* fungus and in determining the concentration of these important vitamins in fungal extracts using chromatography. The $B_6$ vitamers absorb light in the UV region and fluoresce. The absorption spectra of **1**, **2** and **4** are very similar (Fig. 1A). However, the spectrum is red shifted for **3**. This shift is probably due to the electron-withdrawing power of the phosphate and aldehyde groups (Scheme 1), which promote the dissociation of the phenol −OH group in aqueous solutions. In contrast, the pyridoxine spectrum in ethanol is blue shifted by ~38 nm (Table 1). The electron-withdrawing effect is even more pronounced in the fluorescence spectra that are strongly red shifted for **3** (Fig. 1B). Although the absorption spectra of **3** in different solvents are similar (Fig. 2A), the fluorescence intensity is strong in alcohol and the spectrum position is distinct compared to the other pyridoxine derivatives (Fig. 2B). This suggests that the fluorescence of **3** will probably not suffer interference from other forms of the vitamin during fluorescence imaging in the fungus. In preliminary experiments we were able to obtain a fluorescence image from the fungus after incubation with pyridoxal phosphate.

### Quenching of $^1O_2$ phosphorescence

We chose RB as a noninterfering photosensitizer to produce $^1O_2$ for quenching measurements and for pyridoxine oxidation assays because its UV absorption spectrum does not

**Table 1.** Quenching of $^1O_2$ by pyridoxine and derivatives and their oxidation rate by $^1O_2$

| Compound (P) | Buffer or solvent | $k_q \times 10^{-7}$ $M^{-1}$ $s^{-1}$ | Observed oxidation rate of P ($\mu M$ $\times$ $min^{-1}$) | [P]* $\mu M$ | Relative oxidation rate constant ($k_r$(rel) $\times 10^{-3}$) | Extinction coefficient ($M^{-1}$ $cm^{-1}$ $\times 10^{-3}$) | $\lambda_{max}$ (nm) |
|---|---|---|---|---|---|---|---|
| Pyridoxine hydrochloride | pD = 12 | 24.9 ± 0.1 | | | | | |
| | pH = 8.2 | 12.8† | 54.3 | 176 | 77 | 6.32 | 322 |
| | pD = 7.4 | 10.3 ± 0.6‡ | | | | | |
| | pH = 7.2 | 9.6† | 30.6 | 123 | 59 | 6.50 | 322 |
| | pH = 6.3 | 6.3† | 35.9 | 168 | 51 | 6.29 | 322 |
| | pD = 6.1 | 5.51 ± 0.04 | | | | | |
| Pyridoxine free base | Ethanol | 0.345 ± 0.003 | 5.4 | 202 | 2.1 | 5.87 | 286 |
| Pyridoxal hydrochloride | pD = 12 | 60.27 ± 0.02 | | | | | |
| | pH = 8.2 | 12.9† | 27.8 | 70 | 94 | 7.63 | 316 |
| | pD = 8 | 10.01 ± 0.06 | | | | | |
| | pH = 7.2 | 8.5† | 13.2 | 55 | 56 | 8.61 | 316 |
| | pD = 7.4 | 8.70 ± 0.14‡ | | | | | |
| | pH = 6.3 | 7.7† | 10.6 | 65 | 38 | 8.59 | 316 |
| | pD = 6.1 | 7.5 ± 0.2 | | | | | |
| Pyridoxamine dihydrochloride | pH = 8.2 | 10.6 | 38.9 | 72.8 | 125 | 6.85 | 322 |
| | pD = 7.4 | 9.9 ± 0.2‡ | | | | | |
| | pH = 7.2 | 9.7† | 15.5 | 43 | 83 | 7.18 | 322 |
| | pH = 6.3 | 8.9† | 17.7 | 84 | 49 | 7.21 | 322 |
| Pyridoxal 5-phosphate | pD = 12 | 40.0 ± 0.2 | | | | | |
| | pD = 6.1 | 8.79 ± 0.03 | | | | | |
| | pH = 8.2 | 12.2† | 91.2 | 194 | 118 | 4.93 | 388 |
| | pD = 7.4 | 6.2 ± 0.2‡ | | | | | |
| | pH = 7.2 | 5.1† | 36.7 | 164 | 53 | 5.14 | 388 |
| | pH = 6.3 | 5† | 22.2 | 167 | 31 | 4.92 | 388 |

*Concentrations at which the pyridoxine oxidation rates were measured.

†Values estimated from the $k_q$–pH dependence in $D_2O$ and used to calculate the relative oxidation rate constants. Quenching and photooxidation were measured using RB to produce $^1O_2$ in $D_2O$ and $H_2O$ solutions, respectively. In the photooxidation experiments, each time 3.8 mL of solution was used for irradiation. Photooxidation rates were calculated from the absorption spectra using extinction coefficient at the $\lambda_{max}$ after RB absorption spectrum was subtracted. Observed oxidation rate is presented as the decrease in vitamin concentration in μmol per minute of irradiation. Phosphate buffers (50 m$M$) were used in all experiments performed at room temperature in air-saturated solutions. Singlet oxygen lifetime measured in ethanol and water was 14.2 μs and 4.4 μs, respectively. Calculation of relative oxidation rates, $k_4$(rel.), is described in the Materials and Methods.

‡Reported in Ehrenshaft *et al.* (1).

overlap with that of the vitamers, thus making it possible to detect substrate oxidation spectrally. We have found that pyridoxine, pyridoxal, pyridoxal 5-phosphate and pyridoxamine all efficiently quench $^1O_2$ phosphorescence. The total (physical and chemical quenching) rate constant $k_q$ values are in the range of $10^7$–$10^8$ $M^{-1}$ $s^{-1}$ (Fig. 3, Table 1). The quenching was more efficient in alkaline solution but decreased by about one order of magnitude in ethanol when pyridoxine free base was used as a quencher (Table 1). Apparently, the dissociation of the –OH group in water and in alkaline solution produces the phenoxy anion that is a stronger $^1O_2$ quencher than phenols. However, the higher rate constant of $^1O_2$ quenching in water compared to ethanol cannot be due solely to the ionization of the –OH group, because quenching is still faster in water at neutral pH when the –OH group is not dissociated (Table 1). One possible explanation may be that the less polar alcohol solvent may affect internal (resonance) charge distribution in the pyridoxine ring, thereby reducing interaction with $^1O_2$.

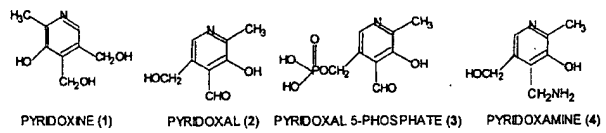


**Scheme 1.**

The quenching of $^1O_2$ is considered to be an additive process involving all active functional groups in a quencher molecule (14). However, the $k_q$ value for pyridoxine is similar to the value for the aldehyde and amino derivatives at similar pH, which suggests that rather than these groups, the aromatic pyridoxine core is the main target for $^1O_2$. Such high reactivity is quite unexpected because other single-ring N-aromatics such as pyridine and most of its derivatives are poorer quenchers of $^1O_2$ with rate constants in the range of $10^5$–$10^6$ $M^{-1}$ $s^{-1}$ (11). Apparently, the substituents in the pyridoxine core and their arrangement facilitate the interaction with $^1O_2$ that can result in the oxidative degradation of vitamin $B_6$ and all its derivatives.

## Oxidation by $^1O_2$

A significant contribution to total quenching by chemical reactions(s) is suggested by the degradation of all $B_6$ vitamers during steady-state irradiation with RB (Fig. 4). The absorption spectra of RB and pyridoxine derivatives do not overlap, allowing selective $^1O_2$ production and a convenient monitoring of photosensitized degradation of pyridoxine *via* its absorption. The vitamin's absorption decreased upon aer-

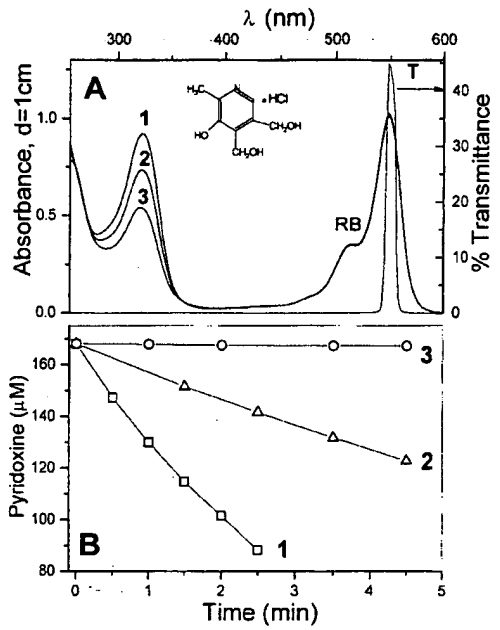


**Figure 4.** Photosensitized degradation of pyridoxine by $^1O_2$. A: Subsequent absorption spectra observed during the irradiation of 0.17 m*M* pyridoxine solutions containing RB; before irradiation (**1**), after 1 min (**2**) and after 2.5 min (**3**) of irradiation. Irradiated solution (3.8 mL) was vigorously stirred with a magnetic bar and air bubbling during irradiation. Transmittance of interference filter used to irradiate RB is shown on the righthand scale. B: Calculated degradation of pyridoxine as a function of irradiation time in the absence of sodium azide (**1**), in the presence of 0.157 m*M* (**2**) and 50 m*M* (**3**) of sodium azide. The initial rate of oxidation from plot **1** was used to calculate the oxidation rate (Table 1).

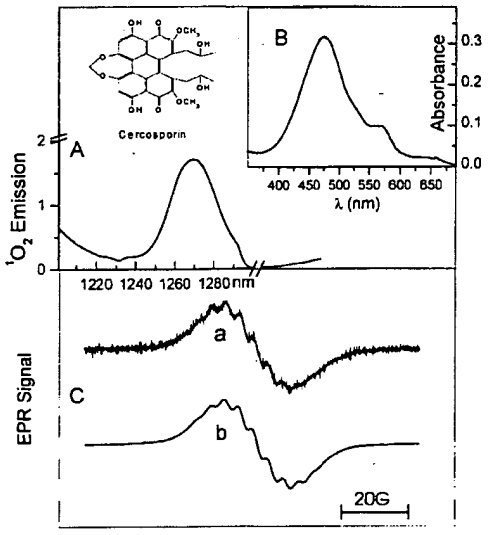


**Figure 5.** Quenching of excited cercosporin by dissolved oxygen and by pyridoxine. A: Spectrum of $^1O_2$ phosphorescence photosensitized in dilute solution of cercosporin in micellar solution of benzalconium chloride illuminated through a 455 num cutoff filter combination in aerobic water and acquired during one 20 s scan. B: The absorption spectrum of cercosporin in benzalkonium chloride (10 m*M*) micelles used to obtain the $^1O_2$ spectrum in A, pathlength 0.5 cm. C: Electron paramagnetic resonance spectrum of cercosporin radical anion (a) produced during the quenching of excited (λ > 400 nm) cercosporin (0.3 m*M*) by pyridoxal 5-phosphate (2 m*M*) in deoxygenated micellar Triton X-100 1% solution at pH 7.4 in phosphate buffer (50 m*M*). Spectrum simulation (b) using the following splitting constants: $a_H(2)$ = 0.86G, $a_H(2)$ = 0.32G and $a_H(4)$ = 0.46G.

ing physical quenching. A closer examination of these values reveals that at physiological pH 7.4, pyridoxamine is most rapidly oxidized, followed by pyridoxine, pyridoxal and pyridoxal 5-phosphate. The oxidation rate decreases slightly at pH 6.3, mostly preserving the same order, which seems to be determined by the substituents' ability to change the electron density in the pyridoxine ring. However, at pH 8.2, the order is reveresed and the oxidation increases, *e.g.* two-fold for pyridoxal 5-phosphate and pyridoxamine (Table 1). This reverse order can be explained by the dissociation of the –OH group producing a phenol anion. The anion may conjugate with the pyridoxine ring, increasing electron density there, which confirms that the core aromatic moiety in the pyridoxine vitamers is a target for the oxidation by $^1O_2$ that interacts more efficiently with electron-rich substrates (17–19).

Our results show that all the pyridoxine vitamers are good substrates for $^1O_2$, because the pyridoxine moiety strongly quenches $^1O_2$ in different chemical environments in which the pyridoxine ring can be rapidly degraded by $^1O_2$. The observation may have serious implications for biological systems, suggesting that $B_6$ vitamers can all be subjected to rapid degradation by $^1O_2$ whenever this species is produced. As vitamin $B_6$ is required for all living cells, degradations by $^1O_2$ may represent an additional mechanism of cellular toxicity by photosensitizers, particularly cells or organisms that do not synthesize pyridoxine but must obtain it from nutritional sources.

### Interaction with the cercosporin photosensitizer

Cercosporin, an endogenous $^1O_2$-generating photosensitizer produced by *Cercospora* fungi, plays an essential role in the ability of this group of filamentous fungi to parasitize plants (20). That $^1O_2$ is generated in fungal culture was recently confirmed spectrally by recording the $^1O_2$ phosphorescence spectrum (25). Although pyridoxine's protective effect in the fungal cell may occur *via* $^1O_2$ quenching, we have also examined whether pyridoxine has the potential to interact directly with cercosporin. The EPR measurements in anaerobic micellar solutions show that pyridoxine quenches the excited cercosporin by donating an electron, as evidenced by an EPR signal from the cercosporin radical anion (Fig. 5C). In the presence of oxygen, no EPR signal was observed, presumably because the production of $^1O_2$ was dominant, indicating that the cercosporin triplet was mostly quenched by dissolved oxygen and not by pyridoxine. We confirmed that $^1O_2$ is efficiently generated (Fig. 5A) by cercosporin in micelles (Fig. 5B). However, at low oxygen concentration, the superoxide radical was detected during the irradiation of cercosporin in dimethylsulfoxide in the presence of pyridoxine and the radical trap DMPO. The superoxide anion is usually produced during photosensitization when oxygen oxidizes the sensitizer radical anion (21).

*Cercospora* fungi appear to use an elaborate system to

protect themselves against oxidative stress induced by cercosporin and other photosensitizers that are highly toxic to other species. One mechanism of defense may be the chemical reduction of cercosporin (22–24) followed by the localization of reduced cercosporin in the aqueous cytoplasm of the cell, an environment that decreases $^1O_2$ production by the reduced derivative (25). Another mechanism may involve pyridoxine as a $^1O_2$ quencher (26). Our data suggest that as a third mechanism, pyridoxine may function as a redox quencher of the cercosporin triplet, leading to superoxide radical production. It is possible that the *Cercospora* fungus may use such reactions to divert cercosporin activation away from the formation of the highly toxic $^1O_2$ to superoxide and other radical forms of oxygen that are better tolerated by living cells.

### Conclusions

Here we have shown that the pyridoxine moiety is a strong quencher of singlet molecular oxygen that initiates rapid oxidation of all $B_6$ vitamers. The $B_6$ vitamers are known to play a required role in cells in enzymatic reactions, primarily in amino acid metabolism, and were not previously implicated in $^1O_2$ or oxidative stress resistance in cells. Our data suggest that pyridoxine and its vitamers can function in photosensitizer resistance by quenching $^1O_2$. Ironically, our results also indicate that $^1O_2$ degrades pyridoxine, an observation that has implications for an additional mode of photosensitizer toxicity to cells, primarily animal cells that do not synthesize pyridoxine but must obtain it through nutritional sources. Our data suggest that oxidative degradation of $B_6$ vitamers can occur during processes in which $^1O_2$ is produced, such as food processing and storage and during photosensitization in the skin. While it is difficult to separate their potential antioxidant properties from the enzymatic role, pyridoxine appears to contribute strongly to the unusual resilience of *Cercospora* fungi to photooxidative stress. Details for the involvement of vitamin $B_6$ in complex processes associated with oxidative stress and whether it can function as an antioxidant in other organisms will require more investigation.

*Acknowledgements*—This work was partially supported by grant MCB-9631375 from the National Science Foundation and grant 96-35303-3204 from the U.S. Department of Agriculture.

## REFERENCES

1. Ehrenshaft, M., P. Bilski, M. Y. Li, C. F. Chignell and M. E. Daub (1999) A highly conserved sequence is a novel gene involved in *de novo* vitamin B6 biosynthesis. *Proc. Natl. Acad. Sci. USA* **96**, 9374–9378.
2. Jenns, A. E., D. L. Scott, E. F. Bowden and M. E. Daub (1995) Isolation of mutants of the fungus *Cercospora nicotianae* altered in their response to singlet-oxygen-generating photosensitizers. *Photochem. Photobiol.* **61**, 488–493.
3. Jenns, A. E. and M. E. Daub (1995) Characterization of mutants of *Cercospora nicotianae* sensitive to the toxin cercosporin. *Phytopathology* **85**, 906–912.
4. Ehrenshaft, M., A. E. Jenns, K. R. Chung and M. E. Daub (1998) *SOR1*, a gene required for photosensitizer and singlet oxygen resistance in *Cercospora* fungi is highly conserved in divergent organisms. *Mol. Cell.* **1**, 603–609.
5. Ehrenshaft, M., K. R. Chung, A. E. Jenns and M. E. Daub (1999) Functional characterization of *SOR1*, a gene required for resistance to photosensitizing toxins in the fungus *Cercospora nicotianae*. *Curr. Genet.* **34**, 478–485.
6. Daub, M. E. (1982) Cercosporin, a photosensitizing toxin from *Cercospora* species. *Phytopathology* **72**, 370–374.
7. Chignell, C. F., P. Bilski, K. Reszka, A. G. Motten, R. H. Sik and T. A. Dahl (1994) Spectral and photochemical properties of curcumin. *Photochem. Photobiol.* **59**, 295–302.
8. Hall, R. D. and C. F. Chignell (1987) Steady-state near infrared detection of singlet molecular oxygen. A Stern–Volmer quenching experiment with sodium azide. *Photochem. Photobiol.* **31**, 37–47.
9. Bilski, P. and C. F. Chignell (1996) Optimization of a pulse laser spectrometer for the measurement of the kinetics of singlet oxygen $O_2(^1\Delta_g)$ decay in solution. *J. Biochem. Biophys. Methods* **33**, 73–80.
10. Bilski, P., L. J. Martinez, E. B. Koker and C. F. Chignell (1996) Photosensitization by norfloxacin is a function of pH. *Photochem. Photobiol.* **64**, 496–500.
11. Wilkinson, F., W. P. Helman and A. B. Ross (1995) Rate constants for the decay and reactions of the lowest electronically excited singlet-state of molecular-oxygen in solution—an expanded and revised compilation. *J. Phys. Chem. Ref. Data* **24**, 663–1021.
12. Duling, D. R. (1994) Simulation of multiple isotropic spin-trap EPR spectra. *J. Magnet. Reson. Ser. B* **104**, 105–110.
13. Dean, J. A. (ed.) (1985) *Lange's Handbook of Chemistry*, 13th ed. McGraw-Hill Book Company, New York.
14. Rodgers, M. A. J. (1983) Solvent-induced deactivation of singlet oxygen: additive relationships in nonaromatic solvents. *J. Am. Chem. Soc.* **105**, 6201–6205.
15. Bilski, P., R. Dabestani and C. F. Chignell (1991) Influence of cationic surfactant on the photoprocesses of eosine and rose bengal in aqueous solution. *J. Phys. Chem.* **95**, 5784–5791.
16. Bilski, P. and C. F. Chignell (1994) Properties of differently charged micelles containing rose bengal: application in photosensitization studies. *Photochem. Photobiol. A Chem.* **77**, 49–58.
17. Bilski, P., A. G. Motten, M. Bilska and C. F. Chignell (1993) The photo-oxidation of diethylhydroxylamine by rose bengal in micellar and nonmicellar aqueous solutions. *Photochem. Photobiol.* **58**, 11–19.
18. Bilski, P., K. Reszka and C. F. Chignell (1994) Oxidation of *aci*-nitromethane by singlet oxygen. *J. Am. Chem. Soc.* **116**, 9883–9889.
19. Bilski, P., K. Reszka, M. Bilska and C. F. Chignell (1996) Oxidation of the spin trap 5,5-dimethyl-1-pyrroline *n*-oxide by singlet oxygen in aqueous solution. *J. Am. Chem. Soc.* **118**, 1330–1338.
20. Daub, M. E., M. Ehrenshaft, A. E. Jenns and K. R. Chung (1998) Active oxygen in fungal pathogenesis of plants: the role of cercosporin in *Cercospora* diseases. In *Phytochemical Signals and Plant–Microbe Interactions, Recent Advances in Phytochemistry*, Vol. 32 (Edited by K. R. Downum and R. Verpoorte), pp. 31–56. Plenum Press, New York.
21. Reszka, K., P. Bilski and C. F. Chignell (1993) Photosensitized generation of superoxide radical in protic solvents: an EPR and spin trapping study. *Free Radical Res. Commun.* **19S**, 33–44.
22. Daub, M. E., G. B. Leisman, R. A. Clark and E. F. Bowden (1992) Reductive detoxification as a mechanism of fungal resistance to singlet-oxygen-generating photosensitizers. *Proc. Natl. Acad. Sci. USA* **89**, 9588–9592.
23. Leisman, G. B. and M. E. Daub (1992) Singlet oxygen yields, optical properties, and photoxicity of reduced derivatives of the photosensitizer cercosporin. *Photochem. Photobiol.* **55**, 373–379.
24. Sollod, C. C., A. E. Jenns and M. E. Daub (1992) Cell surface redox potential as a mechanism of defense against photosensitizers in fungi. *Appl. Environ. Microbiol.* **58**, 444–449.
25. Daub, M. E., M. Li, P. Bilski and C. F. Chignell (2000) Dihydrocercosporin singlet oxygen production and subcellular localization: A possible defense against cercosporin phototoxicity in cercospora. *Photochem. Photobiol.* **71**, *2*, 134–139.
26. Bilski, P., M. Y. Li, M. E. Daub, M. Ehrenshaft and C. F. Chignell (1998) Antioxidant properties of pyridoxine and its derivatives: quenching of singlet oxygen ($^1O_2$). *Free Rad. Biol. Med.*. **25S**, 28.